Published in final edited form as:
Science. 2012 February 24; 335(6071): 966–969. doi:10.1126/science.1213506.

Evolutionarily Assembled cis-Regulatory Module at a Human Ciliopathy Locus

Jeong Ho Lee[1], **Jennifer L. Silhavy**[1], **Ji Eun Lee**[1], **Lihadh Al-Gazali**[2], **Sophie Thomas**[3], **Erica E. Davis**[4], **Stephanie L. Bielas**[1], **Kiley J. Hill**[1], **Miriam Iannicelli**[6], **Francesco Brancati**[6], **Stacey B. Gabriel**[7], **Carsten Russ**[7], **Clare V. Logan**[8], **Saghira Malik Sharif**[8], **Christopher P. Bennett**[8], **Masumi Abe**[9], **Friedhelm Hildebrandt**[10], **Bill H. Diplas**[11], **Tania Attié-Bitach**[3], **Nicholas Katsanis**[4,5], **Anna Rajab**[12], **Roshan Koul**[13], **Laszlo Sztriha**[14], **Elizabeth R. Waters**[15], **Susan Ferro-Novick**[16], **C. Geoffrey Woods**[17], **Colin A. Johnson**[8], **Enza Maria Valente**[6], **Maha S. Zaki**[18], and **Joseph G. Gleeson**[1,*]

[1]Neurogenetics Laboratory, Howard Hughes Medical Institute (HHMI), Department of Neurosciences, University of California, San Diego, CA, USA

[2]Departments of Pediatrics, Faculty of Medicine and Health Sciences, United Arab Emirates University, Al Ain, United Arab Emirates

[3]Département de Génétique, INSERM U781, Hôpital Necker-Enfants Malades, Université Paris Descartes, Paris, France

[4]Center for Human Disease Modeling, Duke University Medical Center, Durham, NC, USA

[5]Department of Cell Biology and Pediatrics, Duke University Medical Center, Durham, NC, USA

[6]Istituto di Ricovero e Cura a Carattere Scientifico Casa Sollievo della Sofferenza, Mendel Laboratory, San Giovanni Rotondo, Italy

[7]Broad Institute of Harvard and Massachusetts Institute of Technology, Cambridge, MA, USA

[8]Department of Clinical Genetics, Yorkshire Regional Genetics Service, St. James's University Hospital, Beckett, UK

[9]Transcriptome Research Center, National Institute of Radiological Sciences, a-shi, Japan

[10]HHMI, Department of Pediatrics, University of Michigan, Ann Arbor, MI, USA

[11]McKusick-Nathans Institute of Genetic Medicine, Johns Hopkins University School of Medicine, Baltimore, MD, USA

[12]Genetic Unit, Directorate General of Health Affairs, Ministry of Health, Muscat, Sultanate of Oman

[13]Department of Child Health (Neurology), Sultan Qaboos University Hospital, College of Medicine and Health Sciences, Muscat, Oman

[14]Department of Pediatrics, Division B, University of Szeged, Szeged, Hungary

[*]To whom correspondence should be addressed: jogleeson@ucsd.edu.

Supporting Online Material
www.sciencemag.org/cgi/content/full/science.1213506/DC1
Materials and Methods
SOM Text
Figs. S1 to S19
Tables S1 to S7
References
Movies S1 to S11

[15]Biology Department, San Diego State University, San Diego, CA, USA

[16]Department of Cellular and Molecular Medicine, HHMI, University of California at San Diego (UCSD), La Jolla, CA, USA

[17]Section of Ophthalmology and Neurosciences, Wellcome Trust Brenner Building, Leeds Institute of Molecular Medicine, St James's University Hospital, Leeds, UK

[18]Clinical Genetics Department, Human Genetics and Genome Research Division, National Research Centre, Dokki, Giza, Egypt

Abstract

Neighboring genes are often coordinately expressed within cis-regulatory modules, but evidence that nonparalogous genes share functions in mammals is lacking. Here, we report that mutation of either *TMEM138* or *TMEM216* causes a phenotypically indistinguishable human ciliopathy, Joubert syndrome. Despite a lack of sequence homology, the genes are aligned in a head-to-tail configuration and joined by chromosomal rearrangement at the amphibian-to-reptile evolutionary transition. Expression of the two genes is mediated by a conserved regulatory element in the noncoding intergenic region. Coordinated expression is important for their interdependent cellular role in vesicular transport to primary cilia. Hence, during vertebrate evolution of genes involved in ciliogenesis, nonparalogous genes were arranged to a functional gene cluster with shared regulatory elements.

Cis-regulatory modules (CRMs) provide binding sites for transcription factors that regulate the expression of neighboring genes (). Relatively little is known about the evolution of these regulatory elements, such as how CRMs arise or how the regulated genes cofunction, other than the rare instance such as *Hox* gene clusters evolved by gene duplication and the addition of regulatory elements to regulate body patterning (2).

Joubert syndrome (JBTS) is the most common neurodevelopmental disorder among the ciliopathy spectrum, which is thought to encompass disorders of structure or function of cellular primary (nonmotile) cilia (3). Affected JBTS patients show hypotonia, ataxia, abnormal eye movement, and a distinct mid-hindbrain malformation presenting the "molar tooth" sign on brain magnetic resonance images (MTI) (fig. S1A) (4). Mounting evidence suggests that primary cilia as cellular antennae sense a wide variety of signals, including Shh signaling, and play a crucial role in vertebrate development (5).

Recently, we reported deleterious mutations of the *transmembrane protein* (*TMEM*) *216* gene, linking to the JBTS2 locus on chromosome 11, in about half of the 10 JBTS2-linked families (Fig. 1A) (6–8). However, the remaining half of the JBTS2 families (verified by the pathognomonic MTI) were phenotypically indistinguishable (displaying optic coloboma, retinal dysplasia, nephronophthisis, and occasional occipital encephalocele) but were negative for mutations in *TMEM216* (fig. S1, A and B, and table S1). Furthermore, fibroblasts from these latter patients contained intact TMEM216 mRNA and protein expression (fig. S2, A and B), thereby suggesting another JBTS causative gene at the JBTS2 locus.

We thus performed resequencing of all known and predicted exonic and promoter genetic elements within the minimal 17-Mb candidate interval defined by *TMEM216* mutation-negative families (9). From these data, we identified four missense mutations and one splicing homozygous deleterious mutation in evolutionarily conserved residues of the nearby *TMEM138* gene of unknown function, thus accounting for all JBTS2-linked families (Fig. 1A, fig. S2C, and table S1). All mutations segregated according to a single recessive disease mode and were not present in 400 ethnically matched chromosomes. Among

missense mutations in transmembrane domains, TMEM138 p.H96R led to unstable protein when transfected into heterologous cells (fig. S2D), suggesting loss of function as the disease mechanism.

Although both *TMEM* genes encode trans-membrane proteins (Fig. 1A), neither the genes nor the proteins demonstrated sequence homology or shared any functional domains. Phylogenetic analysis showed that they represented two distinct protein families, which have evolved separately from invertebrates (figs. S4 and S5), excluding a gene-duplication event. In all higher vertebrates, the two genes aligned in a head-to-tail configuration, with a conserved ~23–kilo–base pair noncoding intergenic interval (Fig. 1B). A synteny map of the genomic locus in a species with deposited reference sequence indicated that they were joined by an ancient chromosomal rearrangement at the amphibian-to-reptile evolutionary transition ~340 million years ago (Fig. 1B and fig. S3). Adjacent genes often exhibit correlated expression (10) and, thus, confer a selective advantage as a genetic module for a certain biological function (11). Therefore, the arrangement of two *TMEM* genes causing indistinguishable phenotypes prompted us to test whether these genes represent co-regulated and cofunctioning genes within a CRM.

To test for coordinated expression, we examined tissue-expression patterns of human *TMEM138* and *TMEM216* using the microarray database and in situ hybridization of human embryos. We found tight coexpression values of human *TMEM138* and *TMEM216* across the major tissues, including the brain and kidneys (fig. S6B), and similar expression patterns in various tissues, including the kidneys, cerebellar buds, and telencephalon, at 4 to 8 gestational weeks (gw) of human embryos (Fig. 2A and fig. S6C). To test whether this coordinated expression was due to the adjacent localization, we compared mRNA levels in zebrafish versus mice, representing species before and after the gene rearrangement event. Using quantitative polymerase chain reaction (qPCR), we detected tightly coordinated expression levels in mice compared with those in zebrafish (correlation coefficient $r = 0.984$ versus 0.386) (Fig. 2B and fig. S6D), which suggests that *TMEM138* and *TMEM216* might share regulatory elements (REs) within the ~23-kb intergenic region. We further examined several experimental features and found that regulatory factor X 4, a transcription factor regulating ciliary genes, binds a RE conserved in the noncoding intergenic region to mediate coordinated expressions of *TMEM138* and *TMEM216* (see SOM text and fig. S7)

The coordinated expression and indistinguishable ciliopathy phenotype caused by either mutation of *TMEM138* and *TMEM216* suggests possible functional relations at the protein level, possibly co-regulating ciliogenesis. We noticed short cilia and failure of ciliogenesis in *TMEM138*-(p.A126T) and *TMEM216*- (p.R73L) mutated fibroblasts, respectively (Fig. 3A), as well as defects of ciliogenesis after knockdown of *TMEM138* and *TMEM216* in IMCD3 cells (fig. S8), suggesting that both TMEM138 and TMEM216 are required for ciliogenesis. Immunostaining of endogenous TMEM138 with a marker (Arl13b) of the ciliary axoneme and transition zone demonstrated closely adjacent localization with TMEM216 at the base of cilia (γ-tubulin), as reported previously (Fig. 3B and fig. S9C) (6). We also noted prominent TMEM138 and TMEM216 adjacent but nonoverlapping vesicular staining around the base of cilia (Fig. 3B and fig. S9, C and D).

Earlier electron-microscopic findings suggested that vesicles transporting to the cilium play a crucial role for targeted delivery of membrane proteins from the Golgi apparatus (12, 13). It is noteworthy that TMEM216 localized to post-Golgi vesicles along microtubules, as well as the Golgi apparatus surrounding the base of cilium, whereas TMEM138 localized to adjacent but nonoverlapping distinct vesicles, shown by immunoelectron microscopic analysis (figs. S10, S11, and S12A). This observation suggests that both TMEM138 and TMEM216 might mark vesicles en route to the base of cilium, which is known to be crucial

for ciliary assembly (14). Using time-lapse analysis with or without fluorescence recovery after photobleaching, we found that the net flux of TMEM216-tagged vesicular movements is toward the centrosome in dsRed-Centrin2 (centrosomal marker) expressing cells (fig. S12B and movies S1 and S2). TMEM138-tagged vesicles displayed tethered vesicular movement with TMEM216-tagged vesicles (fig. S12C and movie S3). This observation prompted us to ask whether the two distinct vesicles differentially carry known ciliary proteins essential for ciliary assembly. We further examined several experimental features showing that TMEM138 and TMEM216 mark two distinct but linked vesicle pools, each associated with unique cilia-targeted proteins, including CEP290 (see SOM text and fig S13).

To understand the adjacency of the two vesicular pools, we tested whether either was required to move vesicles containing the other. Although TMEM216 vesicular movement was not notably affected by disruption of *TMEM138* by small interfering RNA (siRNA), the knockdown of *TMEM216* disrupted the trafficking of TMEM138, as well as CEP290 (figs. S13B and S14, A and B, and movies S5 and S6), suggesting functional dependence on TMEM216 for trafficking TMEM138 and associated proteins.

To determine the mechanism of this functional dependence, we considered the potential role of tethering proteins in linking these two distinct vesicular pools. Several vesicle tethering factors, including the transport protein particle (TRAPP) II complex, p115, and the conserved oligomeric Golgi complex are known to be involved in tethering Golgi vesicles (15). Among these potential tethering proteins, we found that TRAPPII mediated the tethering of TMEM138 and TMEM216 vesicles crucial for ciliary assembly (Fig. 4A, SOM text, figs. S14C to S16, and movies S7 and S8).

We questioned whether the protein localization or mutant phenotype of the two TMEMs in species that diverged before the coordinated gene regulation should be distinct. We found the retention of the coordinated vesicular movement in a zebrafish cell line (ZF4) expressing the tagged version of the two TMEMs zebrafish orthologs, suggesting that the coordinated localization of proteins evolutionarily preceded the coordinated gene expression (movie S11). We next tested for conserved genetic function in zebrafish by comparing the morpholino knockdown phenotypes of each. Both knockdowns shared some typical ciliary phenotypes such as pericardial effusion, a curved or kinked tail (16) in a synergistic and dose-dependent manner, as well as gastrulation defects (Fig. 4B and fig. S18, A to D). However, only *tmem216* morphants presented hydrocephalic brains [ciliary phenotype (17)] and more severe defects of the left/right heart axis (Fig. 4B and figs. S17 and S18A). Together, the data indicate that before their adjacent genomic localization, the proteins' organismal functions were not completely congruent and were associated with distinguishable phenotypes, unlike JBTS2-linked Joubert patients.

Our findings suggest that nonparalogous genes not only can be chromosomally rearranged into a functional gene cluster during vertebrate evolution, but also can be assembled into a new CRM by evolving regulatory elements, which correlate with their coordinated expression. We are aware of few other examples in which mutations in adjacent genes lead to indistinguishable or similar human phenotypes: mutations in *EVC* or *EVC2* cause another ciliopathy, Ellis–van Creveld Syndrome; mutations in *ABCG5* and *ABCG8* cause sitosterolemia; and disruptions of *PKD1* and *TSC2* cause renal cysts (18–20). Our results provide insight into the evolved coordinated expression and functional relatedness of adjacent nonparalogous genes as a pathogenesis of phenotypically indistinguishable genetic disorders caused by mutations at a single locus.

Supplementary Material

Refer to Web version on PubMed Central for supplementary material.

Acknowledgments

We thank the patients and families for invaluable contributions; the Broad Sequencing Plaform, the UCSD Neuroscience Core (grant P30NS047101), and T. Meerloo at the UCSD ImmunoEM Core; M. G. Rosenfeld, B. Ren, P. Novick, K. Frazer, and S. Rifkin for discussion; and C. Janke (Centre de Recherche de Biochimie Macromoléculaire, Montpellier, France, GT335 antibody), T. Caspary (Emory Arl13b antibody), P. Aza-Blanc (Sanford-Burnham Institute, siRNAs), and D. Traver (UCSD) for ZF4 cells. This work was supported by the Daland Fellowship from the American Philosophical Society (J.H.L.), the Italian Ministry of Health (RC2010, Ricerca Finalizzata 2006), Telethon Foundation Italy (GGP08145, E.M.V.), the Pierfranco and Luisa Mariani Foundation (E.M.V.), l'Agence National pour la Recherche (grant ANR-2010-BLAN-1122 01- Foetocilpath, T.A.-B.), the American Heart Association (grant 09POST2250641, J.E.L.), Newlife Foundation for Disabled Children, the Medical Research Council (grant G0700073), the Sir Jules Thorn Charitable Trust (09/JTA, C.A.J.), European Community's Seventh Framework Programme FP7/2009 (241955), SYSCILIA (E.E.D., N.K., C.A.J.), Distinguished George W. Brumley Professorship (N.K.), the NIH (grants NS052455 and NS04843, J.G.G.; DK068306 and DK090917, F.H.; U54 HG003067, E.S. Lander; EY021872, E.E.D.; HD042601, DK075972, DK072301, N.K.), Simons Foundation Autism Research Initiative (J.G.G.), and HHMI (F.H., S.F.-N., J.G.G.).

References and Notes

1. Jeziorska DM, Jordan KW, Vance KW. Semin Cell Dev Biol. 2009; 20:856. [PubMed: 19660565]
2. Manzanares M, et al. Nature. 2000; 408:854. [PubMed: 11130723]
3. Tobin JL, Beales PL. Genet Med. 2009; 11:386. [PubMed: 19421068]
4. Doherty D. Semin Pediatr Neurol. 2009; 16:143. [PubMed: 19778711]
5. Singla V, Reiter JF. Science. 2006; 313:629. [PubMed: 16888132]
6. Valente EM, et al. Nat Genet. 2010; 42:619. [PubMed: 20512146]
7. Keeler LC, et al. Am J Hum Genet. 2003; 73:656. [PubMed: 12917796]
8. Valente EM, et al. Am J Hum Genet. 2003; 73:663. [PubMed: 12908130]
9. Materials and methods are available as supporting material on *Science* Online.
10. Hurst LD, Pál C, Lercher MJ. Nat Rev Genet. 2004; 5:299. [PubMed: 15131653]
11. Stuart JM, Segal E, Koller D, Kim SK. Science. 2003; 302:249. [PubMed: 12934013]
12. Sorokin S. J Cell Biol. 1962; 15:363. [PubMed: 13978319]
13. Papermaster DS, Schneider BG, Besharse JC. Invest Ophthalmol Vis Sci. 1985; 26:1386. [PubMed: 2931395]
14. Nachury MV, Seeley ES, Jin H. Annu Rev Cell Dev Biol. 2010; 26:59. [PubMed: 19575670]
15. Cai H, Reinisch K, Ferro-Novick S. Dev Cell. 2007; 12:671. [PubMed: 17488620]
16. Khanna H, et al. Nat Genet. 2009; 41:739. [PubMed: 19430481]
17. Pathak N, Obara T, Mangos S, Liu Y, Drummond IA. Mol Biol Cell. 2007; 18:4353. [PubMed: 17761526]
18. Ruiz-Perez VL, et al. Am J Hum Genet. 2003; 72:728. [PubMed: 12571802]
19. Berge KE, et al. Science. 2000; 290:1771. [PubMed: 11099417]
20. Kleymenova E, et al. Mol Cell. 2001; 7:823. [PubMed: 11336705]

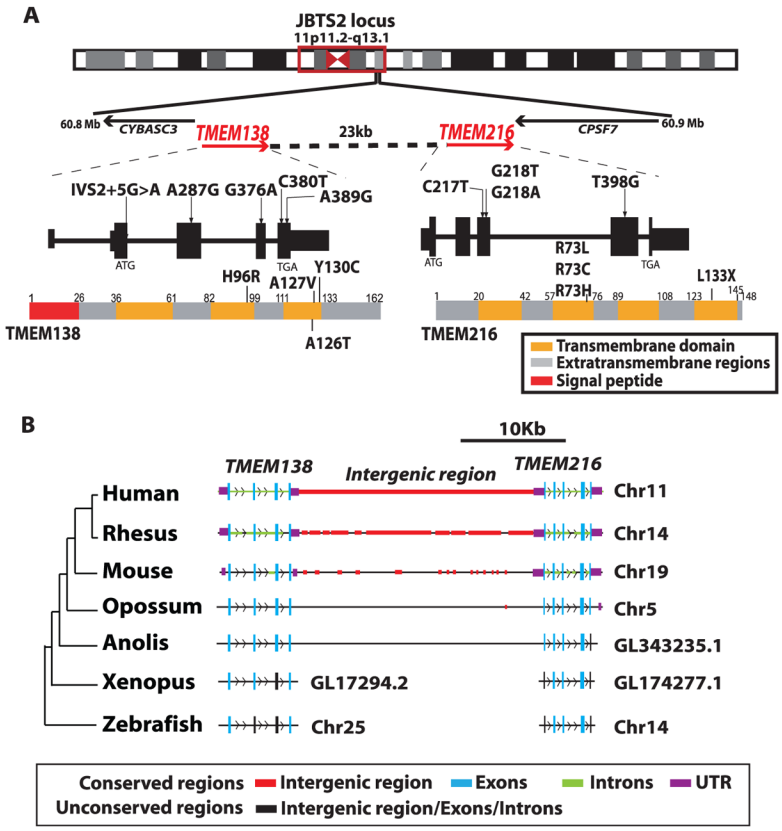

Fig. 1.

Genetic heterogeneity at JBTS2 locus and the evolutionary location of the *TMEM138* and *TMEM216* genes mutated in JBTS2-linked families. (**A**) JBTS2 locus (red box) on chromosome 11. *TMEM138* encoding a trispan membrane protein is aligned in a head-to-tail configuration with *TMEM216* encoding a tetraspan membrane protein. All missense and splicing mutations of *TMEM138* and *TMEM216* found in JBTS2-linked families are indicated on the predicted transcript and protein. (**B**) Schematic synteny representation of *TMEM138*, *TMEM216*, and the intergenic region showing that the head-to-tail configuration of *TMEM138* and *TMEM216* on the same chromosome is conserved from reptiles to humans, but not in lower vertebrates, in which the two *TMEM*s are located on different chromosomes (table S2). Conserved regions have >50% sequence similarity to humans. UTR, untranslated region.

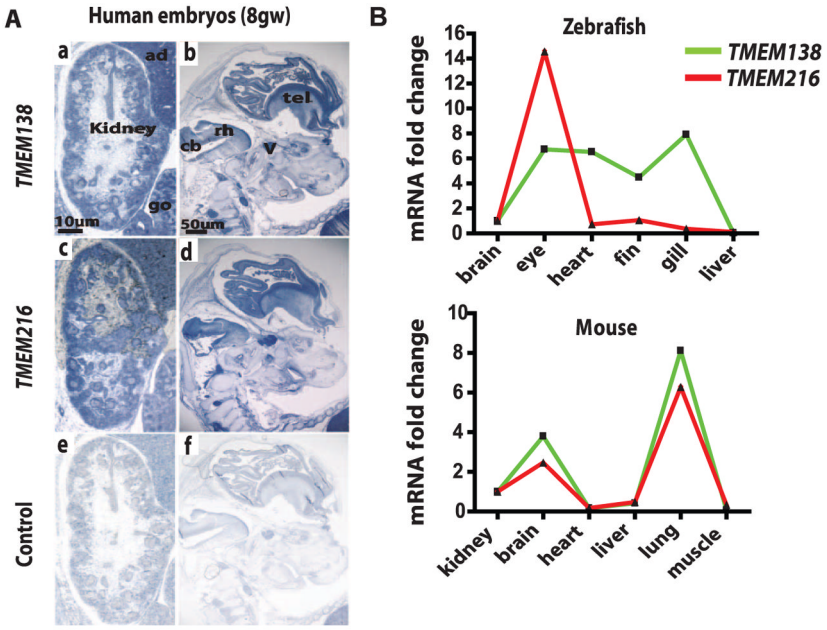

Fig. 2.

Coordinated expression of adjacent *TMEM138* and *TMEM216* mediated by the noncoding intergenic region. (**A**) Similar expression patterns of *TMEM138* and *TMEM216* based on in situ hybridization at 8 gw in human embryonic tissues. *TMEM138* antisense (a and b), *TMEM216* antisense (c and d), and sense control probes (*TMEM138*) (e and f) are shown. *TMEM138* and *TMEM216* are strongly expressed in kidney, gonad (go), and adrenal gland (ad) as well as in the central nervous system, in particular in the cerebellar bud (cb), telencephalon (tel), rhombencephalon (rh), and cranial nerve ganglia such as trigeminal (V). (**B**) Real-time qPCR of *TMEM138* and *TMEM216* in selected tissues indicates tightly coordinated mRNA expressions in mouse tissues (having head-to-tail configuration), but not zebrafish (having two genes on different chromosomes). Housekeeping genes *36B4* (mouse) and *Rpl13a* (zebrafish) are used for normalization.

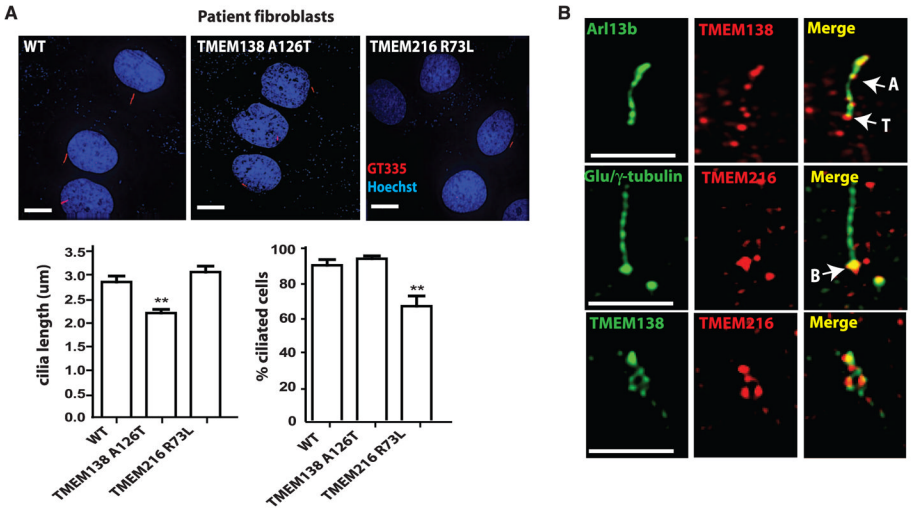

Fig. 3.

Tethered vesicular trafficking of TMEM138 and TMEM216 to primary cilia is required for ciliogenesis. (**A**) In patient fibroblasts under 48-hour serum starvation, TMEM138 p.A126T (MTI-656) mutations caused short cilia, and TMEM216 p.R73L mutations disrupt ciliogenesis (defined as having cilia <1 μm long).*$P < 0.05$, **$P < 0.01$ [versus wild type (WT) by one-way analysis of variance (ANOVA) with Bonferroni posttest, $n = 40$ to 50 cells]. Error bars indicate SEM. (**B**) In IMCD3 cells, high-resolution images of endogenous TMEM138/216 staining show that TMEM138 localized to ciliary axonemes and the base of cilia, whereas TMEM216 localized primarily to basal bodies. Both TMEMs also show closely adjacent vesicular patterns around the base of cilia (also see fig. S9C). Anti-Arl13b (cilia), anti-Glu/γ tubulin (cilia plus centrosome), polyclonal mouse anti-TMEM138 (fig. S9, A and B), and rabbit anti-TMEM216 antibodies were used. A, ciliary axoneme; T, transition zone; B, basal body. Scale bars, 5 μm.

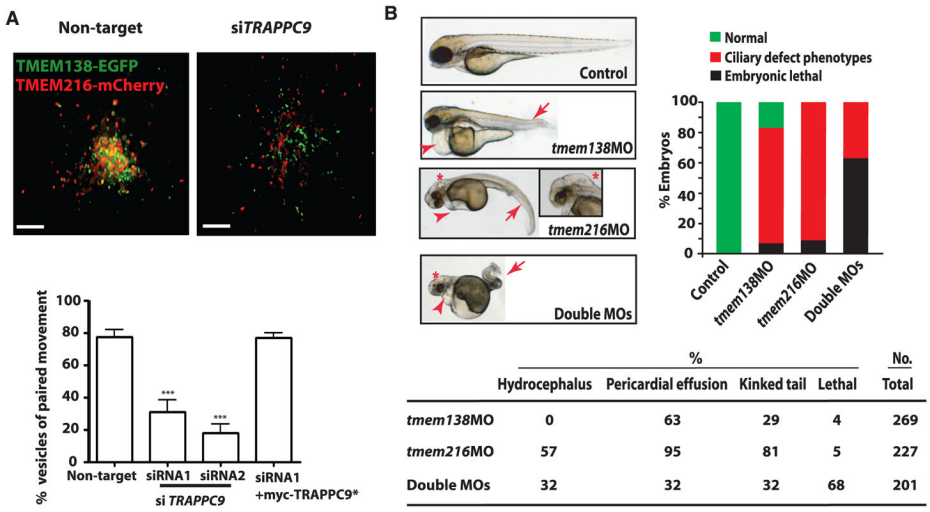

	%				No.
	Hydrocephalus	Pericardial effusion	Kinked tail	Lethal	Total
*tmem138*MO	0	63	29	4	269
*tmem216*MO	57	95	81	5	227
Double MOs	32	32	32	68	201

Fig. 4.

Functional relatedness of TMEM138 and TMEM216. (**A**) Live-cell imaging shows that knockdown of TRAPPC9, a major subunit of the TRAPPII complex, detached the tethered TMEM138 and TMEM216 vesicles (movies S7 and S8). Defects in tethering were largely rescued by myc-*TRAPPC9** (9). ***$P < 0.001$ (by one-way ANOVA with Bonferroni posttest, $n = 90$ to 110). Scale bars, 5 μm. Error bars indicate SEM. (**B**) Injection of translation-blocking antisense morpholinos (MOs) to *tmem138* (6 ng), *tmem216* (4 ng), or double MOs in WT (AB) zebrafish embryos leads to ciliary phenotypes of curved or kinked tail (arrows) and heart edema (arrowheads) at 3 days post-fertilization in a synergistic and dose-dependent manner (fig. S18A). Only *tmem216* morphants present hydrocephalus (*) (>50 embryos for each condition) (fig. S18B).